Chemical Geology 271 (2010) 13–25

Contents lists available at ScienceDirect

Chemical Geology

journal homepage: www.elsevier.com/locate/chemgeo

Detrital zircon U–Pb and Hf isotopic data from the Xigaze fore-arc basin: Constraints on Transhimalayan magmatic evolution in southern Tibet

Fu-Yuan Wu [a,*], Wei-Qiang Ji [a], Chuan-Zhou Liu [a], Sun-Lin Chung [b]

[a] State Key Laboratory of Lithospheric Evolution, Institute of Geology and Geophysics, Chinese Academy of Sciences, P.O. Box 9825, Beijing 100029, China
[b] Department of Geosciences, National Taiwan University, Taipei 106, Taiwan

ARTICLE INFO

Article history:
Received 27 June 2009
Received in revised form 26 November 2009
Accepted 7 December 2009

Editor: R.L. Rudnick

Keywords:
Detrital zircon
U–Pb geochronology
Hf isotope
Xigaze Group
Tibet

ABSTRACT

Before the continental collision of India with Asia, northward subduction of the Tethyan oceanic lithosphere beneath South Asia resulted in widespread arc magmatism in the Lhasa terrane of southern Tibet from Early Jurassic to Eocene time. The detailed magmatic history of this Transhimalayan arc system, however, remains unclear. Here we report *in-situ* detrital zircon U–Pb and Hf isotopic analyses of sedimentary rocks from the Xigaze fore-arc basin, which developed along the southern margin of the Lhasa terrane. The zircon U–Pb results allow us to better constrain the depositional age of the Xigaze Group, which consists from bottom to top of the Chongdui, Ngamring, Padana and Qubeiya formations deposited between ca. 116 and 65 Ma, with the main stage (i.e., the Ngamring Formation) being deposited between ca. 107 and 84 Ma. The majority of these zircons are characterized by high $^{176}Hf/^{177}Hf$ isotopic ratios and positive $\varepsilon_{Hf}(t)$ values that are similar to those of magmatic zircons from the Gangdese batholith, suggesting the latter was a predominant source provenance of the fore-arc sediments. In the younger sequences, i.e., the upper Ngamring and Padana/Qubeiya formations, zircons that record either pre-Mesozoic U–Pb ages or negative $\varepsilon_{Hf}(t)$ values become more abundant, implying additional sources from the northern Lhasa and/or Qiangtang terranes due to northward development of the fluvial systems. The overall zircon U–Pb and Hf isotopic data furthermore suggest that during fore-arc deposition, the exposed Gangdese arc was dominated by igneous rocks formed between 130 and 80 Ma, associated with lesser amounts zircon with ages between 190 and 150 Ma, thus recording two important stages of arc magmatism that are only sporadically preserved in modern outcrops as a result of extensive erosion related to uplift during Mesozoic–Cenozoic time.

1. Introduction

Northward subduction of the Tethyan oceanic lithosphere beneath Asia and the subsequent Indian collision produced the immense Tibetan plateau, which is widely considered to have influenced Asian monsoon circulation, local drainage patterns and global seawater chemistry (e.g., Richter et al., 1992; Molnar et al., 1993). Understanding the Tethyan subduction history, therefore, is vital not only for deciphering the pre-collisional magmatic and tectonic evolution of the region, but also for providing constraints on the initial condition required for any geodynamic models that deal with the key questions such as when and how the Tibetan plateau formed.

North of the Yarlung–Tsangpo suture (Fig. 1), a belt of granitoids that crops out within the Lhasa terrane of southern Tibet for a length of ~2500 km has been termed the "Transhimalayan batholith" (Allègre et al., 1984; Searle et al., 1987; Yin and Harrison, 2000). East of ~80°E, this granitoid belt is represented by the Gangdese batholith or "Gangdese plutonic complex" (Chang and Zheng, 1973; Allègre et al., 1984), from which intrusive magmatism between 190 and 42 Ma has been well documented (cf. Wen et al. (2008) and Ji et al. (2009); for systematic geochronological studies and reviews of the literature age data). Details of the temporal and spatial evolution of Gangdese magmatism, however, remain unknown. The present-day outcrops of the batholith appear to be dominantly composed of Late Cretaceous and Paleogene (ca. 103–42 Ma) granitoids, and those with Jurassic or Early Cretaceous ages are found only as small bodies in limited areas (e.g., Chu et al., 2006; Zhang et al., 2007a). This outcrop pattern is most likely related to extensive erosion caused by topographic uplift before or after the India–Asia collision (Copeland et al., 1987, 1995; Murphy et al., 1997; Kapp et al., 2005, 2007b), which hinders us from directly using the exposed igneous rocks to understand the magmatic evolution of the Gangdese batholith.

Fortunately, Xigaze fore-arc basin sedimentary rocks provide a good opportunity to study the above problem. It is generally accepted that the fore-arc basin is a depression in the sea floor located between an accretionary wedge and an associated volcanic arc in a subduction zone. It is typically filled with thick sedimentary piles derived mainly from the adjacent island arc due to its higher topography (Einsele,

* Corresponding author. Tel.: +86 10 82998217; fax: +86 10 62010846.
E-mail address: wufuyuan@mail.igcas.ac.cn (F.-Y. Wu).

0009-2541/$ – see front matter © 2009 Elsevier B.V. All rights reserved.
doi:10.1016/j.chemgeo.2009.12.007

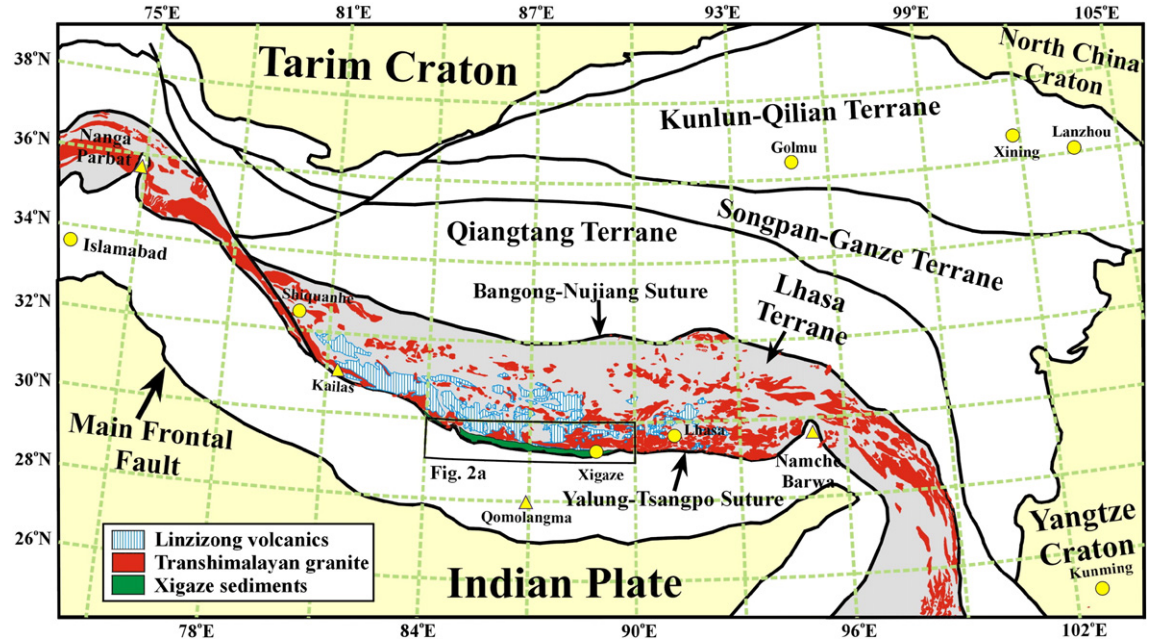

Fig. 1. Simplified geological map of the Tibetan Plateau showing the major units, suture zones and the Transhmalayan granites referred to in the text and the distribution of the Xigaze fore-arc sediments.

2000), suggesting that the fore-arc sediment is a good candidate to decipher the magmatic history of the adjacent arc. The Xigaze fore-arc basin is located at the southern margin of the Lhasa terrane, immediately north of the Yarlung–Tsangpo suture zone (Fig. 1). This basin, composed overwhelmingly of Late Cretaceous clastic sediments sourced from the Gangdese arc complex (Einsele et al., 1994; Dűrr, 1996; Wang et al., 1999), offers a unique opportunity for more quantitative studies of not only the uplift-erosion-deposition relation but also the Mesozoic Gangdese magmatic history. We therefore conducted a combined U–Pb and Lu–Hf isotopic analysis of zircon separates from six sedimentary rocks in the Xigaze basin. Our results, when combined with other recent work in the area (e.g., Chu et al., 2006; Wu et al., 2007; Zhang et al., 2007a; Chiu et al., 2009; Ji et al., 2009), allow us to better constrain the Gangdese magmatic evolution.

2. Geological setting and samples

The Tibetan plateau is composed of the Indian continent in the south and the Asian continent in the north, separated by the Yalung–Tsangpo suture zone (Fig. 1). North of the Yarlung–Tsangpo suture zone, the Lhasa terrane forms part of the Asian continent, with the Cambrian and Precambrian orthogneisses as terrane basement (Guynn et al., 2006). The southern part of the Lhasa terrane is characterized by extensive Jurassic–Early Tertiary calc-alkaline granitoids (Schärer et al., 1984b; Debon et al., 1986; Chung et al., 2005) and Cretaceous to Tertiary non-marine volcanic sequences of the Linzizong Formation (Fig. 1, Maluski et al., 1982; Coulon et al., 1986; Zhou et al., 2004; Chung et al., 2005; He et al., 2007; Lee et al., 2007); whereas the northern Lhasa terrane is characterized by Early Cretaceous volcanic and granitic rocks with formation ages around 100–130 Ma (Coulon et al., 1986; Harris et al., 1988; Kapp et al., 2007a). It is noted that the Early Cretaceous granites in the central-northern Lhasa terrane are mostly peraluminous monzogranites with occurrence of muscovite (S-type?) varieties, which are much different from the hornblende-bearing metaluminous I-type granites in the southern Lhasa terrane. During the Aptian–Albian, the Lhasa terrane was characterized by deposition of shallow-marine limestone and then underwent a transition to non-marine deposition (= Takena equivalent), coeval with the development of major thrust belts in the terrane (northern Lhasa terrane thrust belt in the north and Gangdese retroarc thrust belt in the south) (Murphy et al., 1997; Ding and Lai, 2003; Kapp et al., 2005, 2007b). Further north, the Qiangtang terrane is mostly composed of Paleozoic–Lower Jurassic shallow marine strata with some blueschist and eclogite (Kapp et al., 2000; Li et al., 2006). Cretaceous exposures are limited. It is generally accepted that the Qiangtang terrane was juxtaposed with the Lhasa terrane along the Bangong–Nujiang suture zone which closed during the Middle Jurassic to Early Cretaceous (Allègre et al., 1984; Kapp et al., 2007a).

The Xigaze fore-arc basin extends from Xigaze in the east to Saga in the west, with a length of ~550 km and a width of ~20 km (Fig. 2a). This area has traditionally been defined as a late Early–Late Cretaceous basin consisting mainly of coarse- to fine-grained volcaniclastic sedimentary rocks, with minor intercalated hemi-pelagic marl. Recent geological mapping has indicated that the Xigaze fore-arc basin consists of the Chongdui Formation, and the Xigaze and Tsojiangding groups, deposited during the Cretaceous and Paleocene, respectively (XBGMR, 1997; Jia et al., 2005). The Chongdui (or Congdu or Congdui) Formation, the earliest unit in the Xigaze fore-arc basin, is exposed to south of the Xigaze fore-arc sediment along the Yalung suture. It is in tectonic contact with the ophiolitic mélange in the suture, but locally conformably overlain by the Xigaze Group (Ngamring Formation) (Wu, 1984; Yin et al., 1988; XBGMR, 1997; Wang et al., 1999). As noted below, however, the Chongdui sandstone has the identical zircon U–Pb and Hf isotopic features to samples from the Xigaze Group. Therefore, we consider this formation as the earliest part of the Xigaze Group (Fig. 3). The major rock types of this formation include radiolarian-bearing chert, coarse-grained sandstone, siltstone, mudstone, shale and marly limestone, in which fossils indicate sedimentation during the Albian–Cenomanian (112–94 Ma, Wu, 1984).

The remaining Xigaze Group is divided into the Ngamring, Padana and Qubeiya formations from bottom to top (Fig. 3). The Ngamring Formation was deposited in a deep marine environment and is composed of shale and sandstone, with interlayers and lenses of marly limestone in the lower part, coarse-grained sandstone with thin interlayers of marly limestone and conglomerate in the middle part, and shale with siltstone and limestone layers in the upper part (Wan et al., 1998; Wang et al., 1999; Fig. 4a). The sediments of the Ngamring Formation show a fining-upward trend. The overlying Padana

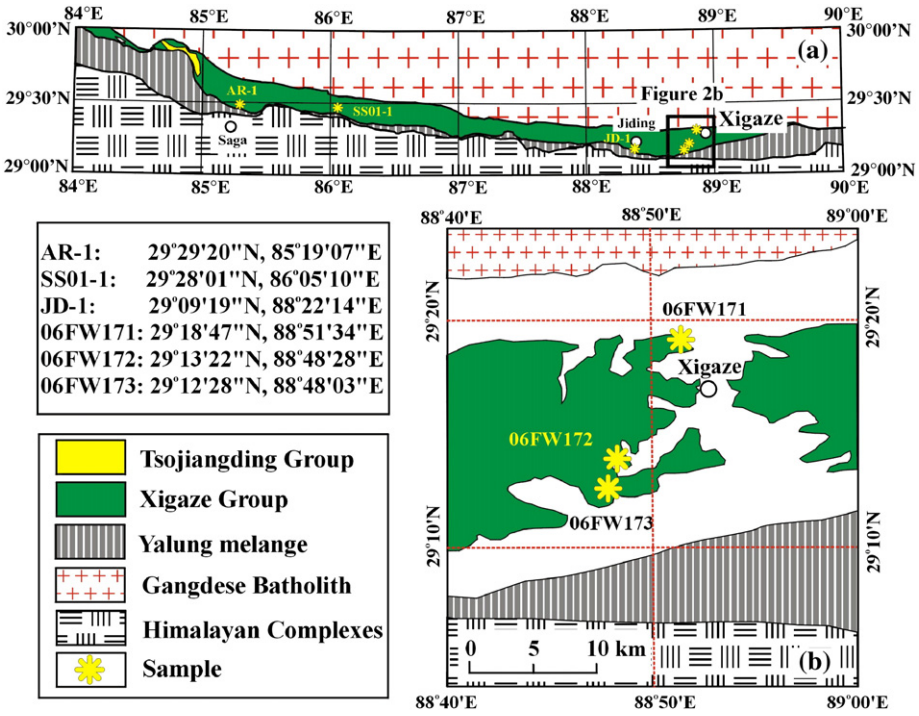

Fig. 2. (a) Geological map showing the locations of samples from the Xigaze fore-arc sediments in this study and, (b) details of the Ngamring Formation near Xigaze City.

Formation is in conformable contact with the Ngamring Formation and is characterized by grey, light green and pink sandstone, mudstone and limestone. The overlying Qubeiya Formation is composed of mudstone and limestone, with interlayers of sandstone. Both the Padana and Qubeiya formations were deposited in a shallow marine environment (Ding et al., 2005). The Tsojiangding Group is located in the western part of the Xigaze basin and unconformably overlies the Xigaze Group (Fig. 3). It can be divided into the basal Quxia Formation (conglomerate dominated) and the overlying Jialazi Formation (Ding et al., 2005), composed of sandstone and conglomerate with grain-size decreasing from base to top. It is proposed that the clastic sediments of this group were deposited in the residual Xigaze fore-arc basin after the India–Asian collision (Ding et al., 2005).

The Ngamring Formation of the Xigaze Group is ~7 km thick (Dűrr, 1996). Based on the metamorphic overprint, shown by the paragenesis of pumpellyite, epidote, titanite, and locally lawsonite in andesitic

Xigaze fore-arc strata

Group	Formation	Main rock types	Samples	
Tsojiangding (Paleogene)	Jialazi	Limestone with sandstone and conglomerate		
	Quxia	Conglomerate and sandstone		65 Ma
Xigaze (Cretaceous)	Qubeiya	Mudstone, limestone and sandstone	AR-01	78 Ma
	Padana	Mudstone, siltstone, sandstone and coarse-grained sandstone, with interlayers of limestone	SS01-1	84 Ma
	Ngamring	Upper: Shale, siltstone, with interlayers of sandstone and limestone	06FW173	
		Middle: Coarse-grained sandstone, with thin layers of limestone	06FW172	
		Lower: Shale, sandstone with interlayers and lenses of limestone	06FW171	107 Ma
	Chongdui	Radiolarian-bearing silicalite, coarse-grained sandstone, siltstone, mudstone with limestone in upper part	JD-1	116 Ma

Fig. 3. Stratigraphic subdivision of the Xigaze Group (modified after XBGMR, 1997; Jia et al., 2005). The age between the Xigaze and Tsojiangding groups is from Ding et al. (2005).

Fig. 4. (a) Occurrence of the Ngamring Formation fore-arc sediments, showing tilting and high relief; (b) sample site of 06FW171, a medium-grained sandstone; (c) sample site of 06FW172, a pebble-bearing coarse-grained sandstone; (d) sample site of 06FW173, a fine-grained sandstone with near vertical bedding.

volcanic clasts, the original thickness of the Ngamring Formation was possibly in the order of 12 km (Dűrr, 1996). The clastic sediments were deposited in deep-sea fans by a variety of gravity processes, including turbidity currents and debris flows (Einsele et al., 1994; Dűrr, 1996; Wang et al., 1999). The southward-trending paleocurrent directions indicate that these sediments were mostly derived from the Asian continent.

Biostratigraphic control is poor because of the predominant flysch-like facies and later metamorphic overprint, resulting in only rare macrofossils and poor preservation of microfossils. The age of the lowest volcaniclastic units in the Xigaze Group is probably Aptian–Albian, as indicated by an upper Albian ammonite, Mortoniceras pricei intermedium, recovered from a stratigraphically intermediate position in the Ngamring Formation (Wiedmann and Durr, 1995). A Coniacian foraminiferal age for the youngest sediments in the Xigaze area has also been obtained (Wan et al., 1998). Therefore, the Xigaze Group was most likely deposited between 86 and 100 Ma. The Qubeiya Formation includes abundant large foraminifera, the species suggesting a late Campanian to late Maastrichtian age (Ding et al., 2005), which is supported by tuff whole-rock Ar/Ar plateau ages of 62.6 ± 0.6 and 62.0 ± 1.0 Ma and zircon U–Pb age of 60.0 ± 2.2 Ma from a volcanic tuff layer in the overlying Tsojingding Group (Ding et al., 2005).

In this study, six samples were collected from the Xigaze Group (Fig. 3). Sample JD-1 was collected south of Jiding, and southwest of Xigaze City (GPS location: N29°09′19″, E88°22′14″). It is a light green, coarse-grained sandstone belonging to the Chongdui Formation. Samples 06FW171 (medium-grained sandstone, GPS location: N29°18′47″, E88°51′34″), 06FW172 (pebble-bearing coarse-grained sandstone, GPS location: N29°13′22″, E88°48′28″) and 06FW173 (fine-grained sandstone, GPS location: N29°12′28″, E88°48′03″) were collected from the Ngamring Formation in the Xigaze area, and represent the lower, middle and upper parts, respectively (Figs. 2b and 3). According to the stratigraphic sub-division of Wan et al. (1998), the above three samples would have been deposited in the Upper Albian, Turonian and Coniacian epochs, respectively. Sample SS01-1 was collected from the Padana Formation (GPS location: N29°28′01″, E86°05′10″) and is a coarse-grained sandstone. Sample AR-1 is a siltstone collected from the Qubeiya Formation, north of Saga (Fig. 2a, GPS location: N29°29′20″, E85°19′07″).

3. Analytical methods

Zircon crystals were obtained from crushed rock using a combination of heavy liquid and magnetic separation techniques. Individual crystals were handpicked, mounted in epoxy resin and polished to remove the upper one third of the grain. Cathodoluminescence (CL) images were obtained using a CAMECA electron microprobe at the Institute of Geology and Geophysics, Chinese Academy of Sciences (IGGCAS) in Beijing, in order to identify internal structures and choose potential target sites for U–Pb and Hf analyses. The working conditions during the CL imaging were at 15 kV. Isotopic measurements were carried out at the MC-ICPMS laboratory of the IGGCAS. An Agilent 7500a quadrupole (Q)-ICPMS and a Neptune multi-collector (MC)-ICPMS were used for simultaneous collection of U–Pb isotopes, trace elements and Lu–Hf isotopes with an attached 193 nm excimer ArF laser-ablation system (GeoLas Plus). During analyses, the ablated aerosol was carried by helium and split into two transport tubes using a three-way pipe and therefore simultaneously introduced into the Q-ICPMS and MC-ICPMS. The proportion of ablated material carried into the two instruments was controlled by three mass flow controllers. Our experiments indicate that there is no significant mass fractionation when different proportions of ablated material were carried into the Q-ICPMS and MC-ICPMS. The detailed analytical procedure, similar to those described by Yuan et al. (2008), can be found in Xie et al. (2008), and only a brief description is given here.

The Agilent 7500a Q-ICPMS has an abaxial Omega II lens system. Under normal operating mode, the sensitivity is better than 20 Mcps/ppm for ^{89}Y, using a 100 μL/min PFA nebulizer and Scott spray chamber. In the case of laser ablation, the sensitivity of ^{238}U in NIST SRM 610 is 14000 cps/ppm using a spot size of 40 μm with laser repetition rate of 10 Hz and laser energy density of 25 J/cm^2. The mass stability is better than 0.05 amu/24 h.

The GeoLas PLUS 193 nm excimer ArF laser ablation system consists of a COMPex 102 ArF excimer laser generator with wavelength of 193 nm, laser optical system with a laser beam homogenizing system,

and Geolas standard software. The highest possible energy density on the sample is 35 J/cm^2, but only 15 J/cm^2 was used in this study. Helium was used as the carrier gas to enhance transport efficiency of the ablated material. The sample cell has a diameter of ~5.8 cm and height of 1.5 cm. This large cell yields a response time of ~10 s, defined as the time the signal takes to decay by a factor of 10 (Wang et al., 2009).

All the gas lines were purged for over 1 h prior to each analytical session to reduce Pb on the surface to ^{204}Pb<50 cps in the gas blank. The measurements were carried out using time resolved analysis operating in a fast, peak hopping sequence in DUAL detector mode. Raw count rates for ^{29}Si, ^{204}Pb, ^{206}Pb, ^{207}Pb, ^{208}Pb, ^{232}Th and ^{238}U were collected for age determination. ^{202}Hg is usually <10 cps in the gas blank, therefore the contribution of ^{204}Hg to ^{204}Pb is negligible and is not considered further. The integration time for the four Pb isotopes was 62.76 ms, whereas for the other isotopes (including ^{29}Si, ^{232}Th and ^{238}U) it was 30 ms. Data were acquired over 30 s with the laser off and 40 s with the laser on, giving ca. 340 (=170 reading/replicate×2 sweeps) mass scans for a penetration depth of ca. 20 μm. The average gas blank is typically <4000 cps for ^{29}Si; <10 cps for ^{204}Pb, ^{206}Pb, ^{207}Pb and ^{208}Pb; <1 cps for ^{232}Th and ^{238}U.

Before analysis, the sample surface was cleaned with ethanol to eliminate possible contamination. Every 10 sample analyses were followed by measurements of one zircon 91500, one TEMORA-2 and one NIST SRM 610. ^{207}Pb/^{206}Pb and ^{206}Pb/^{238}U ratios were calculated using GLITTER 4.0 (Jackson et al., 2004; Griffin et al., 2008), which was then corrected using the Harvard zircon 91500 as an external standard. The ^{207}Pb/^{235}U ratio was calculated from the values of ^{207}Pb/^{206}Pb and ^{206}Pb/^{238}U (^{235}U=^{238}U/137.88). The relative standard deviations of reference values for 91500 were set at 2%. Common Pb was corrected according to the method proposed by Anderson (2002). The weighted mean U–Pb ages and concordia plots were processed using ISOPLOT 3.0. Analyses of the Australian National University zircon standard TEMORA-2 as an unknown yielded a weighted ^{206}Pb/^{238}U age of 416±2 Ma (2σ, n=50), which is in good agreement with the recommended value (Black et al., 2003).

The Neptune MC-ICPMS was used in this study for zircon Hf isotopic measurements. This machine is a double focusing multi-collector ICP-MS and has the capability of high mass resolution measurements in multiple collector mode. The JMC 475 standard solution with 200 ppb Hf was used for evaluating the reproducibility and accuracy of the instrument before laser ablation analyses. The details of this solution measurement can be found in Wu et al. (2006). The results of ^{176}Hf/^{177}Hf for JMC475 Hf standard solution in a long term give an average ^{176}Hf/^{177}Hf ratio of 0.282158±16 (n=140, 2SD) normalized to ^{179}Hf/^{177}Hf=0.7325 using an exponential law for mass bias correction (Wu et al., 2006). This value is identical to that recommended by Nowell et al. (1998). During laser ablation analyses, the isobaric interference of ^{176}Lu on ^{176}Hf is negligible due to the extremely low ^{176}Lu/^{177}Hf in zircon (normally <0.002). However, the interference of ^{176}Yb on ^{176}Hf must be carefully corrected since the contribution of ^{176}Yb to ^{176}Hf could profoundly affect the accuracy of the measured ^{176}Hf/^{177}Hf ratio. In this project, the mean ^{173}Yb/^{171}Yb ratio of the individual spots was used to calculate the fractionation coefficient (β_{Yb}), and then to calculate the contribution of ^{176}Yb to ^{176}Hf. It is shown that this method can provide an accurate correction of the ^{176}Yb interference on ^{176}Hf (Woodhead et al., 2004; Wu et al., 2006; Kemp et al., 2009). During analysis, an isotopic ratio of ^{176}Yb/^{172}Yb=0.5887 was applied (Wu et al., 2006). Standard zircon 91500 was used for external correction. During analytical sessions, the obtained ^{176}Hf/^{177}Hf value of 91500 was 0.282301±8 (2σ), which was adjusted to 0.282305 (correction of 0.000004), a standard value recommended for 91500 (Wu et al., 2006), although it is similar to the values obtained by the solution method, within error (Wiedenbeck et al., 1995; Amelin et al., 2000; Woodhead et al., 2004; Nebel-Jacobsen et al., 2005; Davis et al., 2005). During data acquisition, analyses of TEMORA-2 as an unknown yielded a weighted ^{176}Hf/^{177}Hf ratio of 0.282673±5 (2σ, n=50), identical to the recommended value within error (Wu et al., 2006).

A potential problem during analysis and data processing is the complex age and isotopic structures of the targeted zircons. However, as a specifically designed program in U–Pb analysis, GLITTER can display a time-resolved signal in which the down-hole variation (depth profile) in age is clearly recognizable, and the different zones can be dated separately; described by Jackson et al. (2004) and Griffin et al. (2008). Similarly, Hf isotopic profiles can be also established during laser ablation (Woodhead et al., 2004).

4. Analytical results

All U–Pb data obtained in this study are listed in the electronic supplement as Table A1 in the supplementary material. For statistical purposes, zircons >1000 Ma with discordance <10% and <1000 Ma

Table 1
Summarized characteristics of samples from the Xigaze fore-arc basin.

Sample	Maximum depositional age (Ma)[a]	Major age peak[a]	Percentage of the Mesozoic zircons	Mesozoic zircons with positive $\varepsilon_{Hf}(t)$ value
AR01-1 (n=77) (Qubeiya)	78	78 (n=4), 88 (n=8), **100 (n=15)**, 111 (n=13), 115 (n=11), 124 (n=8), 1160 (n=3), 1806 (n=3)	69% (53 out of 77)	92% (49 out of 53)
SS01-1 (n=75) (Padana Fr.)	93	93 (n=7), **98 (n=8)**, 142 (n=3), 617 (n=3), 656 (n=3), 873 (n=4), 1056 (n=4), 1089 (n=4), 1187 (n=3), 1805 (n=3)	32% (24 out of 75)	50% (12 out of 24)
06FW173 (n=68) (Upper Ngamring Fr.)	88	88 (n=3), **98 (n=4)**, 120 (n=3), **160 (n=5)**, 528 (n=3), 587 (n=3), 691 (n=4), 780 (n=3), 848 (n=3), 909 (n=6), 1147 (n=3), 1190 (n=4), 1283 (n=3), 1744 (n=3)	35% (24 out of 68)	63% (15 out of 24)
06FW172 (n=75) (Middle Ngamring Fr.)	101	101 (n=19), 106 (n=20), **164 (n=34)**	99% (74 out of 75)	100% (74 out of 74)
06FW171 (n=71) (Lower Ngamring Fr.)	107	**107 (n=31)** 128 (n=5)	89% (63 out of 71)	97% (61 out of 63)
JD-1 (n=89) (Chongdui Fr.)	116	**116 (n=74)** 188 (n=4) 200 (n=3)	100% (89 out of 89)	100% (89 out of 89)

[a] The age statistics are conducted by Age Pick program of the Arizona University (http://www.geo.arizona.edu/alc/Analysis%20Tools.htm). The numbers in bold are the most important peak in the sample.

with discordance <20% were considered as usable. The Hf isotopic data are listed in the electronic supplement as Table A2. For clarity, the summarized characteristics of the individual samples are provided in Table 1. For age statistics, Age Pick program of the University of Arizona (Arizona LaserChron website of http://www.geo.arizona.edu/alc/Analysis%20Tools.htm) was used. Representative zircon cathodoluminescence (CL) images from all formations are shown in Fig. 5.

4.1. Chongdui Formation

Zircons from sample JD-1 are stubby to elongate and variable in size, with an average length of ~100 μm; they show oscillatory zoning under CL (Fig. 5a). Eighty-nine usable $^{206}Pb/^{238}U$ ages obtained from 100 analyses show that sample JD-1 of the Chongdui Formation contains exclusively Mesozoic zircons (Figs. 6 and 7a). These include (1) a zircon grain with the oldest $^{206}Pb/^{238}U$ age of 202 ± 5 Ma; (2) six grains with Jurassic ages from 199 ± 7 to 145 ± 11 Ma; and (3) the remaining eighty-two grains of Early Cretaceous age from 105 ± 5 to 139 ± 6 Ma. Statistically, the overall age spectrum shows a large, broad peak centred on ~116 Ma, coupled with a small cluster around 202–182 Ma (Fig. 7a, Table 1). Moreover, all these Mesozoic zircons display high $^{176}Hf/^{177}Hf$ isotopic ratios of 0.282846–0.283179 that yield positive $\varepsilon_{Hf}(t)$ values of +6.5–+17.4 (Fig. 8a and b).

4.2. Ngamring Formation

Zircons from sample 06FW171 of the lower Ngamring Formation (Fig. 4b) show some variations in size, with the largest grains having a length of ~250 μm, but most of them are <100 μm in length. In CL images, most zircons show oscillatory zoning (Fig. 5b). The larger crystals are euhedral with length/width ratios of 1:2–1:4. However, the small zircon grains are usually rounded, perhaps implying a longer transport distance from their source. Ninety-nine zircon grains were analyzed and 71 usable ages were obtained (Fig. 6). The youngest age is 95 ± 2 Ma, with discordance of 9.5%, and other younger ages include 96 ± 4, 97 ± 2 and 98 ± 3 Ma, with discordance of 16%, 4% and −4%, respectively. There are also eight grains showing Precambrian ages, and the oldest one is 1425 ± 15 Ma with a discordance of −0.2%. Most

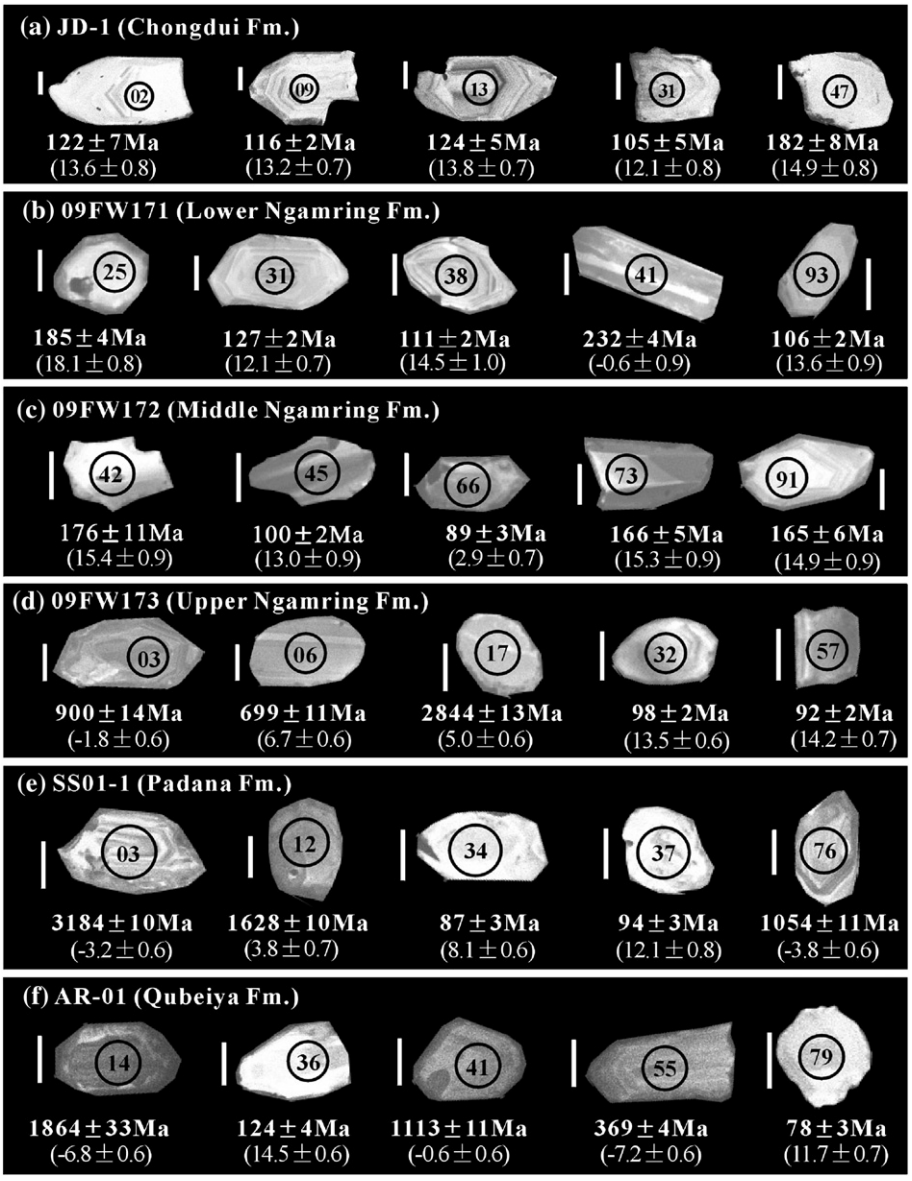

Fig. 5. Representative cathodoluminescence (CL) images of zircons from the Xigaze fore-arc sediments. Scale bar = 50 μm. (a) JD-1 (Chongdui Formation), (b) 06FW171 (lower Ngamring Formation), (c) 06FW172 (middle Ngamring Formation), (d) 06FW173 (upper Ngamring Formation), (e) SS01-1 (Padana Formation) and (f) AR-01 (Qubeiya Formation).

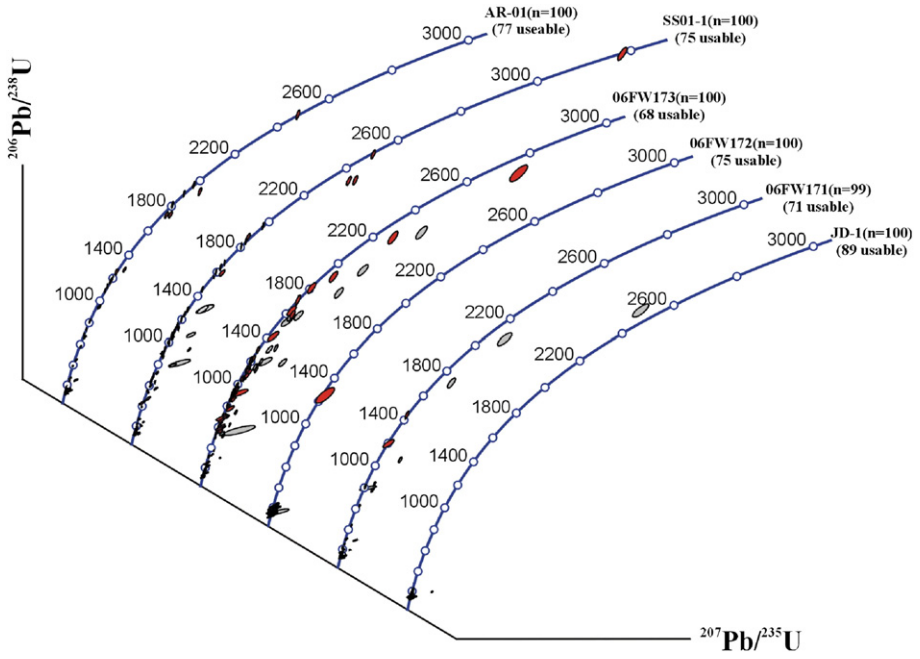

Fig. 6. Compound U–Pb concordia diagrams of samples collected from the Xigaze Group. Ages are in Ma and ellipses show 1σ errors. The names of individual samples, number of analyses, and number of ages that were of sufficient concordance to be used in the study are noted next to the Concordia curve. Analyses in grey are highly discordant, hence are not included in the discussion.

of the zircons (58 out of 71 results, i.e., ~82%) are Cretaceous, with ages ranging from 95 to 143 Ma and the main peak at 107 and a minor peak at 128 Ma (Fig. 7b, Table 1). In terms of Hf isotope composition, the Precambrian zircons display a large variation in $^{176}Hf/^{177}Hf$ isotopic ratios (Fig. 8c), but the Cretaceous zircons show mainly high $^{176}Hf/^{177}Hf$ isotopic ratios and positive $\varepsilon_{Hf}(t)$ values (Fig. 8d).

Zircons from sample 06FW172, collected from the middle Ngamring Formation (Fig. 4c), show somewhat different U–Pb and Hf isotopic characteristics. These zircons are mostly uniform in grain-size with length/width ratios of 1:1–1:3, and most do not show oscillatory zoning but are bright in CL images (Fig. 5c). Among the 75 usable ages from 100 analyses, almost all zircons are Mesozoic except for one Precambrian grain that has $^{207}Pb/^{206}Pb$ age of 1239 ± 45 Ma (Fig. 6). The youngest $^{206}Pb/^{238}U$ ages obtained are 88 ± 11 and 89 ± 3 Ma. The Mesozoic zircons form two age groups of 135–88 and 192–145 Ma, with peaks at ~101, 106 and 164 Ma, respectively (Fig. 7c, Table 1). All Mesozoic zircons display high $^{176}Hf/^{177}Hf$ isotopic ratios and positive $\varepsilon_{Hf}(t)$ values (Fig. 8e and f).

Sample 06FW173 from the upper Ngamring Formation (Fig. 4d) shows a more complex age pattern. Unlike the stratigraphically lower samples, zircons here are mostly rounded with length/width ratios of 1:1–1:2. Some large crystals have a length of ~200 μm with length/width ratios of ~1:3. In CL images, most zircons show banded internal structures (Fig. 5d). Among the 68 usable ages from 100 analyses (Fig. 6), there are "only" 24 Mesozoic zircons with the youngest recording an age of 77 ± 3 Ma and the next two youngest ages are 86 ± 3 and 88 ± 2 Ma (Table 1). These Mesozoic zircons show numerous age groups that, in the order of relative abundance, cluster around 125–80, 170–140 and 240–220 Ma with the main peaks at 88, 98, 120 and 160 Ma, respectively (Fig. 7d, Table 1). In contrast to previous samples, this sample has a large proportion of old zircons that yield numerous small age peaks at 500–1000, 1150–1300 and 1700–1800 Ma (Fig. 7d). It is also noted that in this sample all large crystals yielded Precambrian ages. Along with the highly heterogeneous Hf isotope composition of the old zircons, some of the Mesozoic zircons show high $^{176}Hf/^{177}Hf$ isotopic ratios yielding positive $\varepsilon_{Hf}(t)$ values, whereas others have low $^{176}Hf/^{177}Hf$ ratios and negative $\varepsilon_{Hf}(t)$ values (Fig. 8g and h).

4.3. Padana and Qubeiya formations

Zircons from both the Padana and Qubeiya formations are equal to round in shape and show oscillatory zoning (Fig. 5e and f). Among the 100 zircon analyses of sample SS01-1 from the Padana Formation, 75 concordant and near concordant analyses show a large age range from 87 ± 3 to 3184 ± 10 Ma, with 24 being Mesozoic (Figs. 6 and 7e). These Mesozoic ages form a principal group at 110-80 Ma, with major peaks at 93 and 98 Ma, and a subordinate group of 170–130 Ma with a peak at 142 Ma (Fig. 7e, Table 1). In terms of Hf isotopes, many of the pre-Mesozoic zircons show low $^{176}Hf/^{177}Hf$ isotopic ratios and negative $\varepsilon_{Hf}(t)$ values (Fig. 8i), among which a ~600 Ma grain shows the lowest $\varepsilon_{Hf}(t)$ value of −26.8 ± 0.7. Cretaceous zircons in this sample, similar to the previous samples, possess high $^{176}Hf/^{177}Hf$ isotopic ratios and positive $\varepsilon_{Hf}(t)$ values. However, all except one Jurassic zircon, show low $^{176}Hf/^{177}Hf$ isotopic ratios and negative $\varepsilon_{Hf}(t)$ values (Fig. 8j).

Seventy-seven usable zircon U–Pb analyses were obtained from 100 analyses of sample AR-1, recovered from the Qubeiya Formation north of the Saga township (Fig. 2a). The age data show a wide range from 77 ± 3 to 2480 ± 10 Ma (Fig. 6). Similar to samples from the lower Xigaze Group, there are abundant zircons (i.e., 53 out of 77 analyses, 69%) that record Mesozoic ages, forming an age cluster between ~77 and 129 Ma with major peaks at 78, 88, 100, 111, 115 and 124 Ma (Fig. 7f, Table 1). Most of the pre-Mesozoic zircons have low $^{176}Hf/^{177}Hf$ isotopic ratios and negative $\varepsilon_{Hf}(t)$ values, but the Mesozoic zircons are dominated by high $^{176}Hf/^{177}Hf$ isotopic ratios and positive $\varepsilon_{Hf}(t)$ values (Fig. 8k and l).

5. Discussion

5.1. Depositional constraints on the Xigaze fore-arc basin sediments

The age of the Xigaze Group is poorly constrained because of the general lack of fossils. Biostratigraphic studies suggested that the lowermost part of the Chongdui Formation was deposited during Albian–Cenomanian time (i.e., ca. 112–94 Ma, Wu, 1984), but a more precise age of deposition cannot be provided. It is generally accepted

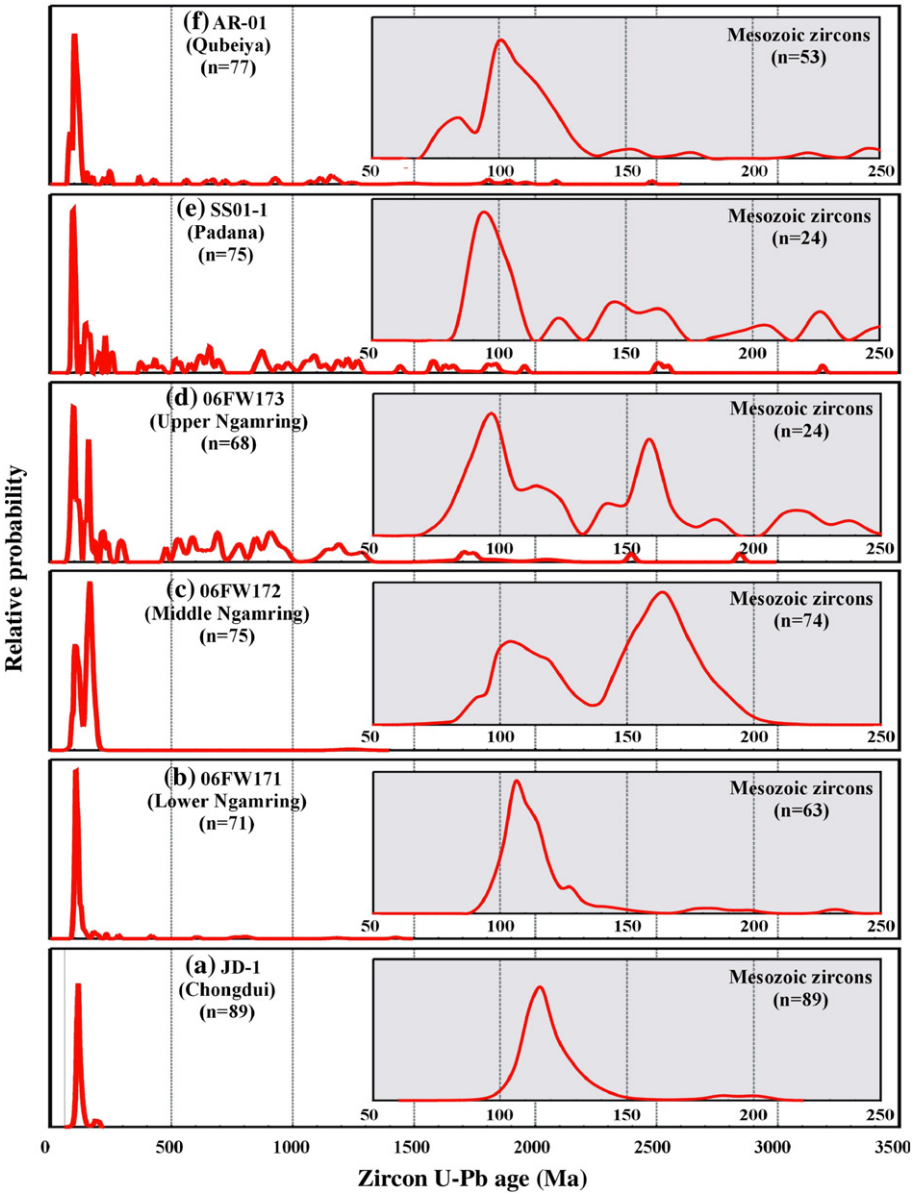

Fig. 7. Relative probability of detrital zircons from the Xigaze Group. For ages <1000 Ma, the $^{206}Pb/^{238}U$ age is used, whereas the $^{207}Pb/^{206}Pb$ age is used for zircon >1000 Ma. (a) JD-1 (Chongdui Formation), (b) 06FW171 (lower Ngamring Formation), (c) 06FW172 (middle Ngamring Formation), (d) 06FW173 (upper Ngamring Formation), (e) SS01-1 (Padana Formation) and (f) AR-01 (Qubeiya Formation).

that the youngest concordant detrital zircon age can be used to constrain the maximum depositional age. If there is both continuous magmatism in the source region and continuous sedimentation in the appropriate depocentre, then this youngest U–Pb age might also be taken to approximate the age of the deposition. This has been demonstrated for Mesozoic strata in the Colorado Plateau (Dickinson and Gehrels, 2009), although more studies are needed to verify this conclusion. Taking the detrital zircon results from our sample JD-1 into account, the youngest ages are 104 ± 7, 105 ± 5, 106 ± 6 and 106 ± 5 Ma. Using the Age Pick program, the youngest peak age is 116 Ma, which provides a conservative lower age limit, suggesting that deposition of the Chongdui Formation, or the entire Xigaze Group, started later than ~116 Ma.

The Ngamring Formation, the major component of the Xigaze Group, is considered to have been deposited from the Late Albian to Late Coniacian (ca. 100–86 Ma), based on microfossils (Wan et al., 1998). According to the biostratigraphic correlation, our samples 06FW171 and 06FW173, collected from the basal and uppermost parts, respectively, of the formation, may be used to approximately constrain the onset and cessation ages of sedimentation. In sample 06FW171, the youngest reliable ages are 95 ± 2, 96 ± 4, 97 ± 2 and 98 ± 3 Ma, with the youngest peak at 107 Ma, similar to that of sample 06FW172 from the middle Ngamring Formation. These age data indicate that the Ngamring Formation might have been deposited slightly later than, but not earlier than, ~107 Ma. Sample 06FW173 from the upper Ngamring Formation has a youngest peak zircon age of 91 Ma. The overlying Padana sample SS01-1 records a youngest zircon age of 80 ± 2 Ma and youngest peak of 84 Ma, which is slightly younger, within error, than the latest depositional age constrained by fossils. We therefore propose that sedimentation in the Ngamring Formation occurred between ca. 107 and 84 Ma, which supports our previous assumption that the youngest U–Pb age of detrital zircon can approximate the age of deposition in an active environment such as the Xigaze fore-arc basin.

The age criteria described above for sample SS01-1 from the Padana Formation imply deposition started around 84 Ma. The

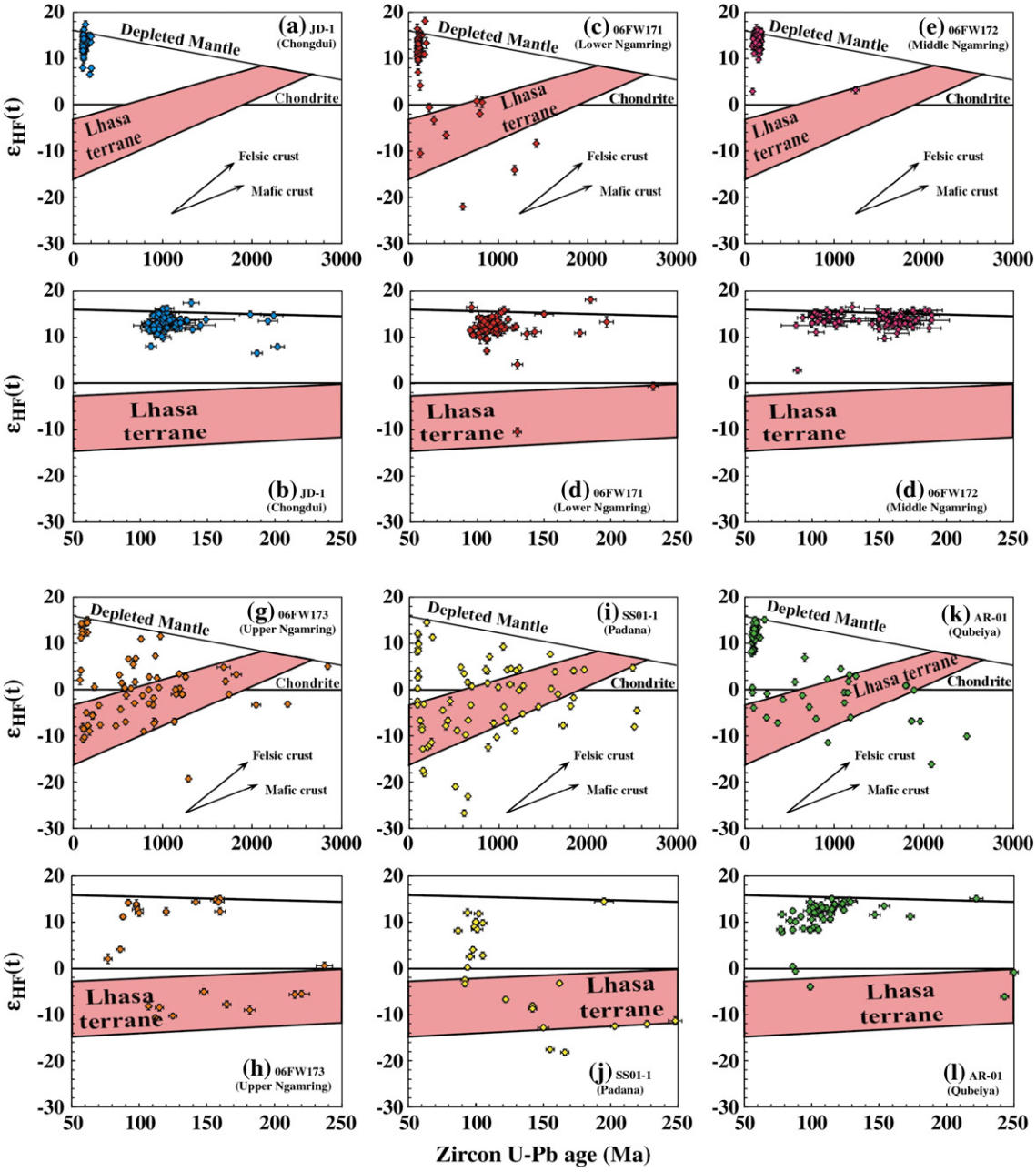

Fig. 8. Hf isotopic features of detrital zircons from the Xigaze Group. The Mesozoic zircons are characterized by positive $\varepsilon_{Hf}(t)$ values in samples of JD-1 (a and b), 06FW171 (c and d), 06FW172 (e and f) and AR-1 (k and l). However, some of the Mesozoic zircons in samples 06FW173 (g and h) and SS01-1 (i and j) share the similar characteristics with those of the Lhasa terrane. Field of the Lhasa terrane is after Chu et al. (2006), Zhang et al. (2007b) and Wu et al. (2007). The error of zircon U–Pb ages is 1σ, but is 2σ for $\varepsilon_{Hf}(t)$ values.

youngest zircon ages in sample AR-1 from the overlying Qubeiya Formation are 77 ± 3, 78 ± 2 and 78 ± 3 Ma, with the youngest peak age at 78 Ma. However, it is interesting to note that this sample is from an outcrop that was originally classified as belonging to the Ngamring Formation by the field mapping team, at odds with the biostratigraphic study (Jia et al., 2005) that reported the Campanian–Masstrichtian (84–65 Ma) fossils in this formation. Our zircon results lend support to the latter view and allow us to conclude that the outcrop is part of the Qubeiya Formation, the youngest formation of the Xigaze Group, in which deposition started after ~78 Ma.

To sum up, the sedimentary sequences of the Xigaze Group were deposited essentially in Late Cretaceous time, commencing with the Chongdui Formation after ~116 Ma, followed by the Ngamring Formation between ~107 and 84 Ma, and ending with the Padana and Qubeiya formations between ~84 and 65 Ma.

5.2. Sources of the Xigaze sediments

It is generally considered that sediments in the Xigaze basin were mainly derived from the Gangdese batholith, or associated Transhimalayan volcanic successions (Einsele et al., 1994; Dűrr, 1996). Besides, the carbonate shelf in the fore-arc region may have served as another important source of the sediments. Dűrr (1996), based on the identification of a large amount of quartz, rutile and chromite in the sandstones within the fore-arc basin, proposed that these minerals are sourced from the Bangong–Nujiang suture or Qiangtang terrane in the north (Fig. 1), brought by southward-flowing rivers across the Gangdese batholith. This implies that the Gangdese batholith was not yet a high mountain range during the Late Cretaceous when the fore-arc basin formed. The similarity between the age peaks in this study and the ages obtained from the granites in the northern Lhasa terrane

seems support this conclusion (Murphy et al., 1997; Volkmer et al., 2007).

In the Himalayan–Tibetan orogenic belt, the combined analysis of zircon U–Pb and Lu–Hf analysis has proven to be a very useful tool for studying not only the petrogenesis of the Gangdese arc rocks (e.g., Chu et al., 2006; Lee et al., 2007; Zhang et al., 2007a; Chiu et al., 2009; Ji et al., 2009), but also the sedimentary "source-to-sink" relation of the surrounding basins (e.g., Wu et al., 2007; Liang et al., 2008). Zircon Hf isotopic data available for the Gangdese batholith are characterized by high $^{176}Hf/^{177}Hf$ isotopic ratios that yield positive, juvenile mantle-type $\varepsilon_{Hf}(t)$ values. These include Triassic–Jurassic (Chu et al., 2006; Zhang et al., 2007a; Ji et al., 2009), and voluminous Cretaceous to Paleogene granitoids (Chu et al., 2006; Chu, 2006; Liang et al., 2008; Ji et al., 2009; Chiu et al., 2009; Chu et al., in preparation). In contrast, to the north of the Gangsede arc, zircons from Mesozoic granites from the northern plutonic belt in the northern Lhasa terrane have significantly lower $^{176}Hf/^{177}Hf$ ratios and exclusively negative $\varepsilon_{Hf}(t)$ values (Chu et al., 2006; Zhang et al., 2007b; Zhou et al., 2008). For example, Zhang et al. (2007b) reported that the Late Triassic (202 ± 1 and 205 ± 1 Ma) granites in the Central Lhasa terrane have negative zircon $\varepsilon_{Hf}(t)$ values of -12.4 to -1.8 with an average of -6.1 ± 0.7 (2σ). The inherited Jurassic zircons from Cretaceous granites in the area reveal similar $\varepsilon_{Hf}(t)$ values of -13.8–-4.9 (average aof-7.8 ± 0.9), except for a single grain of Early Cretaceous zircon that has a slightly positive $\varepsilon_{Hf}(t)$ value of $+0.9$ (Chu et al., 2006). The latter is similar to the zircon $\varepsilon_{Hf}(t)$ values ($+1.3\pm0.4$, $n=15$) reported by Zhou et al. (2008) for an Early Cretaceous granite in the same area. All these available data indicate that zircons from the granitoids in the central Lhasa terrane, or the southern part of the voluminous northern plutonic belt, have much lower and mostly negative $\varepsilon_{Hf}(t)$ values relative to those of the Gangdese batholith to the south.

Although workers (Kapp et al., 2005, 2007a,b; Volkmer et al., 2007) have recently reported age results documenting that early Cretaceous granites are widespread in the northern Lhasa terrane, there are scarce Hf isotope data available for these zircons. A recent study of the Bangge pluton (113 ± 1 Ma) in this area yielded zircon $\varepsilon_{Hf}(t)$ values of -6.1–$+0.1$ with an average of -3.9 ± 0.5 (Zhu, D.-C., 2009, personal communication), which is consistent with the negative $\varepsilon_{Nd}(t)$ values of Cretaceous granites in the same area (Harris et al., 1988). Therefore, the limited amount of data implies that Cretaceous zircons from the northern Lhasa terrane are also characterized, if not dominated, by negative $\varepsilon_{Hf}(t)$ values. With the understanding that further analyses are required to substantiate this conclusion, the zircon Hf isotopic evidence described above does not support the notion that the Xigaze sediments have a major source provenance from the northern Lhasa terrane. This conclusion is consistent, or at least not at odds, with the paleocurrent data reported for the Cretaceous Takena Formation (Leier et al., 2007a), which was deposited in the back-arc north of the Gangdese, coeval with sedimentation in the Xigaze basin to the south. The paleocurrent data indicate that the Takena sedimentary sequences have a southern rather than northern source (Leier et al., 2007a), implying that during the Late Cretaceous, the Gangdese arc was a topographic high that may have served as a major source provenance for both the Takena basin in the north and the Xigaze basin in the south.

In the present study, 327 out of 455 (~72%) zircons analyzed from all samples are Mesozoic in age. We note that most of the Mesozoic zircons are elongate with length/width ratios of 1:2–1:3 and show oscillatory zoning, typical of an igneous origin. As shown in Fig. 9a, a majority of these Mesozoic zircons record positive $\varepsilon_{Hf}(t)$ values that plot into the Gangdese arc field, thus showing the Gangdese Hf isotopic signature. The zircon data lead us to conclude that the Gangdese arc is the main provenance source of the Xigaze fore-arc sediments. However, a smaller fraction of Mesozoic zircons showing negative $\varepsilon_{Hf}(t)$ values are also present and these plot in or around the Lhasa terrane range, as defined by zircons from the northern plutonic belt (Fig. 9a). This, together with the presence of ~28% (i.e., 128 out of

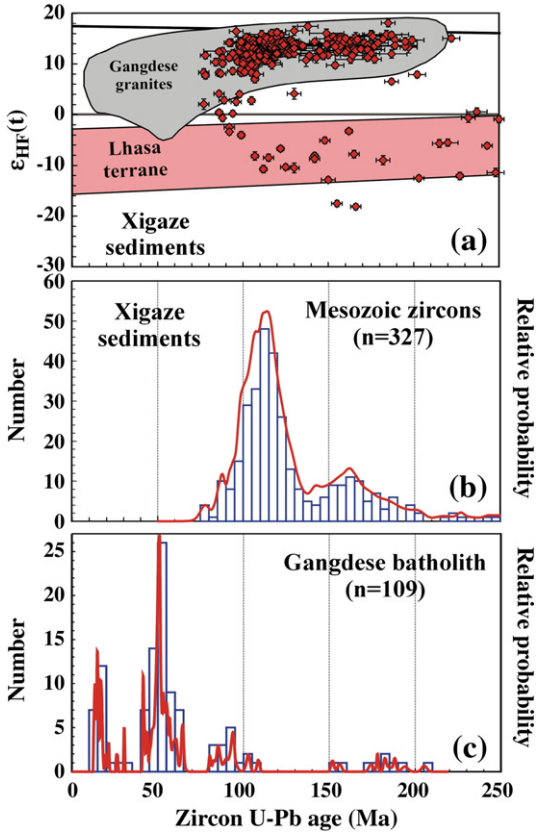

Fig. 9. (a) Detrital zircon Hf isotopic characteristics and compared with those from the Gangdese batholith; both are characterized by positive $\varepsilon_{Hf}(t)$ values. Fields of the Lhasa terrane and Gangdese batholith are after Chu et al. (2006), Zhang et al. (2007a,b), Wu et al. (2007) and Ji et al. (2009); (b) Relative probability diagram of the U–Pb ages of detrital zircons from the Xigaze sediments, showing a prominent age range at 130–80 Ma and a weaker range at 190–150 Ma; (c) Relative probability diagram of zircon U–Pb ages of the Gangdese batholith (After Ji et al., 2009).

a total of 455 analyses) pre-Mesozoic zircons, suggest additional, yet less substantial, sources that include Mesozoic igneous rocks in the northern Lhasa terrane and the basement rocks in the Lhasa or even Qiangtang terranes (Leier et al., 2007b). More specifically, there are temporal variations in terms of zircon U–Pb ages and Hf isotopes (Figs. 7 and 8). The detrital zircons in the lowest formation (i.e., Chongdui Formation; sample JD-1) are 100% Mesozoic (Fig. 7a), with predominantly Early Cretaceous ages and subordinate Jurassic–Triassic ages (Fig. 7a); and all these zircons show high positive $\varepsilon_{Hf}(t)$ values (Fig. 8a) that imply the Gangdese arc was the only source of detritus at this stage. Later, during deposition of the Ngamring and younger formations (Figs. 7 and 8), not only did the amount of Jurassic–Triassic zircons increase significantly, but together with pre-Mesozoic zircons with negative $\varepsilon_{Hf}(t)$ values also increased. In particular, a dramatic change occurred between the middle and upper Ngamring Formations (Fig. 7c and d), allowing the suggestion that the fluvial systems may have cut across the Gangdese mountains and started linking to the north. Hence, igneous and basement rocks in the northern Lhasa and/or Qiangtang terranes became additional sources of sediment for the upper Ngamring, and Padana and Qubeiya Formations.

5.3. Magmatic evolution of the Gangdese arc during the Mesozoic

The zircon U–Pb and Lu–Hf isotope data suggest that during formation of the Xigaze fore-arc, i.e., between ca. 116 and 65 Ma, the outcrop of the Gangdese arc complex was dominantly composed of rocks formed during two magmatic episodes. These are, as illustrated

in Fig. 9b, a principal magmatic stage between ~130–80 Ma (peaking at ~110 Ma) and a subordinate stage between ~190–150 Ma (peaking at ~160 Ma). This age distribution pattern, however, differs markedly from that of present-day exposures of the Gangdese batholith in which both the Early Cretaceous and Jurassic rocks are observed only in limited localities and as small bodies (Fig. 9c, and see below).

Since the pioneering Sino-French joint study (Schärer et al., 1984a,b), the Gangdese batholith has been repeatedly investigated with respect to its emplacement age and magmatic evolution by a number of workers (e.g., Murphy et al., 1997; Harrison et al., 2000; McDermid et al., 2002; Mo et al., 2005; Chung et al., 2005; Dong et al., 2005; Chu et al., 2006; Xia et al., 2007; Mo et al., 2007; Wen et al., 2008; Chiu et al., 2009; Ji et al., 2009). Among these, Wen et al. (2008), Chiu et al. (2009) and Ji et al. (2009) most recently reported on a geochronological study of the Gangdese batholith that, combined with a synthesis of published age data, allowed them to conclude that the modern Gangdese outcrop consists of two main stages of plutonic rocks, formed during the Late Cretaceous and early Paleogene, respectively. Earlier intrusions did occur, but perhaps only in small areas, such as the Triassic–Jurassic calc-alkaline granites in Wuyu, Nymo and Qulong, which show zircon U–Pb ages between 152 and 205 Ma (Chu et al., 2006; Zhang et al., 2007a; Yang et al., 2008; Ji et al., 2009).

However, along with our present study, two lines of depositional evidence suggest that Mesozoic Gangdese magmatism was more active than is generally acknowledged. Firstly, recent mapping involving detailed field investigations indicate that the Yeba and Sangri Formations, two Mesozoic sedimentary/volcanic successions in the Lhasa terrane, are more widespread than previously thought. Geochronological studies indicate that the Yeba Formation was formed during the Jurassic, with zircon U–Pb ages ranging from 174 to 182 Ma (Geng et al., 2006; Dong et al., 2006; Zhu et al., 2008). Although no reliable age is available for the Sangri Formation, fossil data suggest that this series of volcanic rocks was formed during the early Cretaceous at around 120–110 Ma (Dong et al., 2006). Secondly, detrital zircons from Cretaceous sedimentary rocks in the northern Lhasa terrane are dominated by Mesozoic ages clustering around 160–100 Ma, coupled with a subordinate group at ~180–220 Ma (Leier et al., 2007b). Although it can be argued that some of these sediments were derived from erosion of Mesozoic granites in the northern Lhasa or Qiangtang terranes, paleogeographic reconstruction suggests that they mostly were deposited by north-trending paleocurrents that cut across and eroded the Gangdese batholith (Leier et al., 2007a).

To conclude, despite the fact that modern Gangdese outcrops appear largely composed of Paleogene to Late Cretaceous granitoids, Mesozoic depositional records from both fore-arc and back-arc sides of the Gangdese arc indicate that magmatism was already active and widespread in the Early Cretaceous, and probably since Jurassic–Triassic time. The scarcity of these older igneous rocks in the present Gangdese arc complex is attributed to significant erosion in the region owing to orogenic uplift and erosion. Given that erosion could have greatly changed the Gangdese arc exposures, thus distorting our understanding the magmatic evolution, we emphasise the importance of studying the detrital records that, combined with direct investigation of the exposed Gangdese batholith itself, may provide new insights into our comprehension of its magmatic evolution.

6. Concluding remarks

The combined U–Pb and Hf isotopic analysis of detrital zircons from the Xigaze fore-arc basin, southern Tibet have led to the following major conclusions:

1) The Xigaze Group that consists from bottom to top of the Chongdui, Ngamring, Padana and Qubeiya formations was deposited in a fore-arc basin between ca. 116 and 65 Ma, with the main stage of deposition (i.e., the Ngamring Formation) being formed between ca. 107 and 84 Ma.
2) The Xigaze fore-arc sediments were dominantly derived from erosion of the Gangdese arc, characterized by high $^{176}Hf/^{177}Hf$ isotopic ratios and positive $\varepsilon_{Hf}(t)$ values. Sediments from the northern Lhasa and/or Qiangtang terranes are less abundant and started to contribute to the sediments after deposition of the middle Ngamring Formation.
3) During the Late Cretaceous, when the Xigaze fore-arc basin was forming in southern Tibet, the exposed Gangdese arc was mainly composed of igneous rocks produced in two stages, i.e., a principal stage at ca. 130–80 Ma and a subordinate stage at 190–150 Ma. The limited exposure of both stages of Gangdese rocks at the present time indicates that significant erosion and uplift took place during deposition of the studied sediments or after the India–Asian collision in the Cenozoic.
4) The combined in-situ analysis of U–Pb and Lu–Hf isotopes in detrital zircons is a useful tool for investigating not only the sedimentary source-to-deposition relation but also the magmatic evolution in the Himalayan–Tibetan orogenic belt.

Acknowledgements

We thank Jin-Xiang Li and Feng-Cai Luo for assistance in the fieldwork, Yue-Heng Yang and Jin-Feng Sun for help with the laser ablation analyses. Paul Kapp and Ian Campbell read an early draft and provided many critical suggestions. Constructive comments from Aaron Martin and Tony Kemp improved the paper greatly. This work benefited from financial supports from the Chinese Academy of Sciences (KZCX2-YW-Q09-06-2) and the National Natural Science Foundation of China (NSFC Grant of 40721062).

Appendix A. Supplementary data

Supplementary data associated with this article can be found, in the online version, at doi:10.1016/j.chemgeo.2009.12.007.

References

Allègre, C.J., Courtillot, V., Tapponnier, P., Hirn, A., Mattauer, M., Coulon, C., Jaeger, J.J., Achache, J., Schärer, U., Marcoux, J., Burg, J.P., Girardeau, J., Armijo, R., Gariépy, C., Göpel, C., Li, T.D., Xiao, X.C., Chang, C.F., Li, G.Q., Lin, B.Y., Teng, J.W., Wang, N.W., Chen, G.M., Han, T.L., Wang, X.B., Deng, W.M., Sheng, H.B., Cao, Y.G., Zhou, J., Qiu, H.R., Bao, P.S., Wang, S.C., Wang, B.X., Zhou, Y.X., Xu, R.H., 1984. Structure and evolution of the Himalaya–Tibet orogenic belt. Nature 307, 17–22.

Amelin, Y., Lee, D.C., Halliday, A.N., 2000. Early–middle Archean crustal evolution deduced from Lu–Hf and U–Pb isotopic studies of single zircon grains. Geochim. Cosmochim. Acta 64, 4205–4225.

Anderson, T., 2002. Correction of common lead in U–Pb analyses that do not report ^{204}Pb. Chem. Geol. 192, 59–79.

Black, L.P., Kamo, S.L., Allen, C.M., Aleinikoff, J.N., Davis, D.W., Korsch, R.J., Foudoulis, C., 2003. TEMORA 1: a new zircon standard for Phanerozoic U–Pb geochronology. Chem. Geol. 200, 155–170.

Chang, C.F., Zheng, L.S., 1973. Tectonic features of the Mount Jolmo Lungma region in southern Tibet. China. Sci. Geol. Sin. 1, 1–12.

Chiu, H.Y., Chung, S.L., Wu, F.Y., Liu, D.Y., Liang, Y.H., Lin, I.J., Iizuka, Y., Xie, L.W., Wang, Y.B., Chu, M.F., 2009. Zircon U–Pb and Hf isotopic constraints from eastern Transhimalayan batholiths on the pre-collisional magmatic and tectonic evolution in southern Tibet. Tectonophysics 477, 3–19.

Chu, M.F., 2006. Application of LA-ICPMS in the study of the Transhimalayan petrogenesis, PhD Thesis, National Taiwan University.

Chu, M.F., Chung, S.L., Song, B., Liu, D.Y., O'Reilly, S.Y., Pearson, N.J., Ji, J.Q., Wen, D.J., 2006. Zircon U–Pb and Hf isotope constraints on the Mesozoic tectonics and crustal evolution of Southern Tibet. Geology 34, 745–748.

Chu, M.F., Chung, S.L., O'Reilly, S.Y., Griffin, W.L., Pearson, N.J., Liu, D.Y., Ji, J.Q., in preparation. Reading zircon Hf isotopic code for Tibetan orogenesis, Neotethyan subduction and Gondwana dispersion.

Chung, S.L., Chu, M.F., Zhang, Y.Q., Xie, Y.W., Lo, C.H., Lee, T.Y., Lan, C.Y., Li, X.H., Zhang, Q., Wang, Y.Z., 2005. Tibetan tectonic evolution inferred from spatial and temporal variations in post-collisional magmatism. Earth-Sci. Rev. 68, 173–196.

Copeland, P., Harrison, T.M., Kidd, W.S.F., Xu, R., Zhang, Y., 1987. Rapid early Miocene acceleration of uplift in the Gangdese Belt, Xizang (southern Tibet), and its bearing

on accommodation mechanisms of the India–Asia collision. Earth Planet. Sci. Lett. 86, 240–252.
Copeland, P., Harrison, T.M., Yun, P., Kidd, W.S.F., Royden, M., Zhang, Y., 1995. Thermal evolution of the Gangdese batholith, southern Tibet: a history of episodic unroofing. Tectonics 14, 223–236.
Coulon, C., Maluski, H., Bollinger, C., Wang, S., 1986. Mesozoic and Cenozoic volcanic rocks from central and southern Tibet: ^{39}Ar–^{40}Ar dating, petrological characteristics and geodynamical significance. Earth Planet. Sci. Lett. 79, 281–302.
Davis, D.W., Amelin, Y., Nowell, G.M., Parrish, R.R., 2005. Hf isotopes in zircon from the western Superior province, Canada: implications for Archean crustal development and evolution of the depleted mantle reservoir. Precambrian Res. 140, 132–156.
Debon, F., Le Fort, P., Sheppard, S.M., Sonet, J., 1986. The four plutonic belts of the Transhimalaya–Himalaya: a chemical, mineralogical, isotopic, and chronological synthesis along a Tibet–Nepal section. J. Petrol. 27, 219–250.
Dickinson, W.R., Gehrels, G.E., 2009. Use of U–Pb ages of detrital zircons to infer maximum depositional ages of strata: a test against a Colorado Plateau Mesozoic database. Earth Planet. Sci. Lett. 288, 115–125.
Ding, L., Lai, Q.Z., 2003. New geological evidence of crustal thickening in the Gangdese block prior to the Indo-Asian collision. Chin. Sci. Bull. 48, 1604–1610.
Ding, L., Kapp, P., Wan, X.Q., 2005. Paleocene–Eocene record of ophiolite obduction and initial India–Asia collision, south central Tibet. Tectonic 24. doi:10.1029/2004TC001729.
Dong, G.C., Mo, X.X., Zhao, Z.D., Guo, T.Y., Wang, L.L., Chen, T., 2005. Geochronologic constraints on the magmatic underplating of the Gangdese belt in the India–Eurasia collision: evidence of SHRIMP II zircon U–Pb dating. Acta Geol. Sinica 79, 787–794.
Dong, Y.H., Xu, J.F., Zeng, Q.G., Wang, Q., Mao, G.Z., Li, J., 2006. Is there a Neo-Tethys' subduction record earlier than arc volcanic rocks in the Sangri Group? (in Chinese with English abstract). Acta Petrol. Sin. 22, 661–668.
Dűrr, S.B., 1996. Provenance of Xigaze fore-arc basin clastic rocks (Cretaceous, south Tibet). Geol. Soc. Am. Bull. 108, 669–684.
Einsele, G., 2000. Sedimentary Basins: evolution, facies, and sediment budget, 2nd edition. Springer-verlag, Berlin. 792 pp.
Einsele, G., Liu, B., Dűrr, S., Frisch, W., Liu, G., Luterbacher, H.P., Ratschbacher, L., Ricken, W., Wendt, J., Wetzel, A., Yu, G., Zheng, H., 1994. The Xigaze forearc basin: Evolution and facies architecture (Cretaceous, Tibet). Sed. Geol. 90, 1–32.
Geng, Q.R., Pan, G.T., Wang, L.Q., Zhu, D.C., Liao, Z.L., 2006. Isotopic geochronology of the volcanic rocks from the Yeba Formation in the Gangdise zone, Xizang (in Chinese with English abstract). Sed. Geol. Tethyan Geol. 26, 1–7.
Griffin, W.L., Powell, W.J., Pearson, N.J., O'Reilly, S.Y., 2008. GLITTER: data reduction software for laser ablation ICP-MS. In: Sylvester, P. (Ed.), Laser Ablation-ICP-MS in the Earth Sciences: Current Practices and Outstanding Issues: Mineral. Assoc. Canada Short Course, vol. 40, pp. 308–311.
Guynn, J.H., Kapp, P., Pullen, A., Heizler, M., Gehrels, G., Ding, L., 2006. Tibetan basement rocks near Amdo reveal "missing" Mesozoic tectonism along the Bangong suture, central Tibet. Geology 34, 505–508.
Harris, N.B.W., Xu, R., Lewis, C.L., Hawkeworth, C.J., Zhang, Y., 1988. Isotope geochemistry of the 1985 Tibet Geotraverse, Lhasa to Golmud. Philos. Trans. R. Soc. Lond. A327, 263–285.
Harrison, T.M., Yin, A., Grove, M., Lovera, O.M., Ryerson, F.J., Zhou, X., 2000. The Zedong Window: a record of superposed Tertiary convergence in southeastern Tibet. J. Geophys. Res. 105, 19211–19230.
He, S.D., Kapp, P., DeCelles, P.G., Gehrels, G.E., Heizler, M., 2007. Cretaceous–Tertiary geology of the Gangdese Arc in the Linzhou area, southern Tibet. Tectonophysics 433, 15–37.
Jackson, S.E., Pearson, N.J., Griffin, W.L., Belousova, E.A., 2004. The application of laser ablation-inductively coupled plasma-mass spectrometry (LA-ICP-MS) to *in situ* U–Pb zircon geochronology. Chem. Geol. 211, 47–69.
Ji, W.Q., Wu, F.Y., Chung, S.L., Li, J.X., Liu, C.Z., 2009. Zircon U–Pb geochronological and Hf isotopic constraints on petrogenesis of the Gangdese batholith in Tibet. Chem. Geol. 262, 229–245.
Jia, J.C., Wei, C.S., Wang, G.H., Zhang, Z.L., Wang, L.J., 2005. New understanding of stratum of Xigaze forearc basin in the north of Qiongguo area, Zhongba, Tibet (in Chinese with English abstract). N.W. Geol. 38 (2), 33–39.
Kapp, P., Yin, A., Manning, C.E., Murphy, M., Harrison, T.M., Spurlin, M., Ding, L., Deng, X. G., Wu, C.M., 2000. Blueschist-bearing metamorphic core complexes in the Qiangtang block reveal deep crustal structure of northern Tibet. Geology 28, 19–22.
Kapp, P., Yin, A., Harrison, T.M., Ding, L., 2005. Cretaceous–Tertiary shortening, basin development, and volcanism in central Tibet. Geol. Soc. Am. Bull. 117, 865–878.
Kapp, P., DeCelles, P.G., Gehrels, G.E., Heizler, M., Ding, L., 2007a. Geological records of the Cretaceous Lhasa–Qiangtang and Indo-Asian collisions in the Nima basin area, central Tibet. Geol. Soc. Am. Bull. 119, 917–932.
Kapp, P., DeCelles, P.G., Leier, A.L., Fabijanic, J.M., He, S.D., Pullen, A., Gehrels, G.E., 2007b. The Gangdese retroarc thrust belt revealed. GSA Today 17 (7), 4–9.
Kemp, A.I.S., Foster, G.L., Scherstén, A., Whitehouse, M.J., Darling, J., Storey, C., 2009. Concurrent Pb–Hf isotope analysis of zircon by laser ablation multi-collector ICP-MS, with implications for the crustal evolution of Greenland and Himalayas. Chem. Geol. 261, 244–260.
Lee, H.Y., Chung, S.L., Wang, Y.B., Zhu, D.C., Yang, J.H., Song, B., Liu, D.Y., Wu, F.Y., 2007. Age, petrogenesis and geological significance of the Linzizong volcanic successions in the Linzhou basin, southern Tibet: evidence from zircon U–Pb dates and Hf isotopes (in Chinese with English abstract). Acta Petrol. Sin. 23, 493–500.
Leier, A.L., Kapp, P., DeCelles, P.G., Ding, L., 2007a. The Takena Formation of the Lhasa terrane, southern Tibet: the record of a Late Cretaceous retro-arc foreland basin. Geol. Soc. Am. Bull. 119, 31–48.
Leier, A.L., Kapp, P., Gehrels, G.E., DeCelles, P.G., 2007b. Detrital zircon geochronology of Carboniferous–Cretaceous strata in the Lhasa terrane, southern Tibet. Basin Res. 19, 361–378.
Li, C., Zhai, Q.G., Dong, Y.S., Huang, X.P., 2006. Discovery of eclogite and its geological significance in Qiangtang, central Tibet. Chin. Sci. Bull. 31, 1095–1100.
Liang, Y.H., Chung, S.L., Liu, D.Y., Xu, Y.G., Wu, F.Y., Yang, J.H., Wang, Y.B., Lo, C.H., 2008. Detrital zircon evidence from Burma for reorganization of the eastern Himalayan river system. Am. J. Sci. 308, 618–638.
Maluski, G., Proust, F., Xiao, X.C., 1982. $^{39}Ar/^{40}Ar$ dating of the trans-Himalayan calc-alkaline magmatism of southern Tibet. Nature 298, 152–154.
McDermid, I.R.C., Aitchison, J.C., Davis, A.M., Harrison, T.M., Grove, M., 2002. The Zedong terrane: a Late Jurassic intra-oceanic magmatic arc within the Yarlung–Tsangpo suture zone, southeastern Tibet. Chem. Geol. 187, 267–277.
Mo, X.X., Dong, G.C., Zhao, Z.D., Guo, T.Y., Wang, L.L., Chen, T., 2005. Timing of magma mixing in Gangdise magmatic belt during the India–Asia collision: zircon SHIRMP U–Pb dating. Acta Geol. Sinica 79, 66–76.
Mo, X.X., Hou, Z.Q., Niu, Y.L., Dong, G.C., Qu, X.M., Zhao, Z.D., Yang, Z.M., 2007. Mantle contributions to crustal thickening during continental collision: evidence from Cenozoic igneous rocks in southern Tibet. Lithos 96, 225–242.
Molnar, P., England, P., Martinod, J., 1993. Mantle dynamics, the uplift of the Tibetan plateau, and the Indian monsoon. Rev. Geophys. 31, 357–396.
Murphy, M.A., Yin, A., Harrison, T.M., Durr, S.B., Chen, Z., Ryerson, F.J., Kidd, W.S.F., Wang, X., Zhou, X., 1997. Did the Indo-Asian collision along create the Tibetan plateau? Geology 25, 719–722.
Nebel-Jacobsen, Y., Scherer, E.E., Munker, K., Mezger, K., 2005. Separation of U, Pb, Lu, and Hf from single zircons for combined U–Pb dating and Hf isotope measurements by TIMS and MC-ICPMS. Chem. Geol. 220, 105–120.
Nowell, G.M., Kempton, P.D., Noble, S.R., Fitton, J.G., Saunders, A.D., Mahoney, J.J., Taylor, R.N., 1998. High precision Hf isotope measurements of MORB and OIB by thermal ionisation mass spectrometry: insights into the depleted mantle. Chem. Geol. 149, 211–233.
Richter, F.M., Rowley, D.B., DePaolo, D.J., 1992. Sr isotope evolution of seawater: the role of tectonics. Earth Planet. Sci. Lett. 109, 11–23.
Schärer, U., Hamet, J., Allègre, C.J., 1984a. The Transhimalaya Gangdese plutonism in the Ladakh region: a U–Pb and Rb–Sr study. Earth Planet. Sci. Lett. 67, 327–339.
Schärer, U., Xu, R.H., Allègre, C.J., 1984b. U–Pb geochronology of Gandese (Transhimalaya) plutonism in the Lhasa-Xigaze region Tibet, Earth Planet. Sci. Lett. 69, 311–320.
Searle, M.P., Windley, B.F., Coward, M.P., Coward, M.P., Rex, A.J., Li, T.D., Xiao, X.C., Jan, M.Q., Thakur, V.C., Kumar, S., 1987. The closing of Tethys and the tectonics of the Himalaya. Geol. Soc. Am. Bull. 98, 678–701.
Volkmer, J.E., Kapp, P., Guynn, J.H., Lai, Q., 2007. Cretaceous–Tertiary structural evolution of the north central Lhasa terrane, Tibet. Tectonics 26, TC6007. doi:10.1029/2005TC001832.
Wan, X.Q., Luo, W., Wang, C.S., Luba, J.S., 1998. Discovery and significance of Cretaceous fossils from the Xigaze forearc basin, Tibet. J. Asian Earth Sci. 16, 217–223.
Wang, C.S., Liu, Z.F., Li, X.H., Wan, X.Q., 1999. Xigaze fore-arc basin and Yarlung Zangbo suture zone, Tibet (in Chinese with English abstract). Geological Publishing House, Beijing. 237 pp.
Wang, C.Y., Campbell, I.H., Allen, C.M., Williams, I.S., Eggins, S.M., 2009. Rate of growth of the preserved North American continental crust: evidence from Hf and O isotopes in Mississippi detrital zircons. Geochim. Cosmochim. Acta 73, 712–728.
Wen, D.R., Liu, D.Y., Chung, S.L., Chu, M.F., Ji, J.Q., Zhang, Q., Song, B., Lee, T.Y., Yeh, M.W., Lo, C.H., 2008. Zircon SHRIMP U–Pb ages of the Gangdese batholith and implications for Neotethyan subduction in southern Tibet. Chem. Geol. 252, 191–201.
Wiedenbeck, M., Alle, P., Corfu, F., Griffin, W.L., Meier, F., Oberli, F., Von Quadt, A., Roddick, J.C., Spiegel, W., 1995. Three natural zircon standards for U–Th–Pb, Lu–Hf, trace element, and REE analyses. Geostand. Newsl. 19, 1–23.
Wiedmann, J., Durr, S., 1995. First ammonites from the Mid- to Upper Cretaceous Xigaze Group, South Tibet, and their significance. Newsl. Stratigraphy 32, 17–26.
Woodhead, J., Hergt, J., Shelley, M., Eggins, S., Kemp, R., 2004. Zircon Hf-isotope analysis with an excimer laser, depth profiling, ablation of complex geometries, and concomitant age estimation. Chem. Geol. 209, 121–135.
Wu, H.R., 1984. The Congdu Formation–Cretaceous deep-sea deposits in southern Xizang (Tibet) and its significance (in Chinese with English abstract). Sci. Geol. Sin. No. 1, 26–33.
Wu, F.Y., Yang, Y.H., Xie, L.W., Yang, J.H., Xu, P., 2006. Hf isotopic compositions of the standard zircons and baddeleyites used in U–Pb geochronology. Chem. Geol. 234, 105–126.
Wu, F.Y., Clift, P.D., Yang, J.H., 2007. Zircon Hf isotopic constraints on the sources of the Indus Molasse, Ladakh Himalaya, India. Tectonics 26, TC2014. doi:10.1029/2006TC002051.
XBGMR (Xizang Bureau of Geology and Mineral Resources), 1997. Regional lithostrata of Tibet (in Chinese with English abstract). China Uni. Geosci. Press, Wuhan, pp. 240–244.
Xia, B., Wei, Z.Q., Zhang, Y.Q., Xu, L.F., Li, J.F., Wang, Y.B., 2007. SHRIMP U–Pb zircon dating of granodiorite in the Kangrinboqe pluton in western Tibet, China and its geological implications (in Chinese with English abstract). Geol. Bull. Chin. 26, 1014–1017.
Xie, L.W., Zhang, Y.B., Zhang, H.H., Sun, J.F., Wu, F.Y., 2008. *In situ* simultaneous determination of trace elements, U–Pb and Lu–Hf isotopes in zircon and baddeleyite. Chin. Sci. Bull. 53, 1565–1573.
Yang, Z.M., Hou, Z.Q., Xia, D.X., Song, Y.C., Li, Z., 2008. Relationship between western porphyry and mineralization in Qulong copper deposit if Tibet and its enlightenment to further exploration (in Chinese with English abstract). Mineral Dep. 27, 28–36.
Yin, A., Harrison, T.M., 2000. Geologic evolution of the Himalayan–Tibetan orogen. Annu. Rev. Earth Planet. Sci. 28, 211–280.
Yin, J.X., Wen, C.F., Sun, Y.Y., 1988. Congdui Formation—the strata of the Late Jurassic to early Late Cretaceous trench-slope basin in Yarlung Zangbo suture zone (in Chinese). Bull. Inst. Geol., Chin. Acad Sci. No. 3, 119–129.

Yuan, H.L., Gao, S., Dai, M.N., Zong, C.L., Günther, D., Fontaine, G.H., Liu, X.M., Diwu, C.R., 2008. Simultaneous determinations of U–Pb age, Hf isotopes and trace element compositions of zircon by excimer laser-ablation quadrupole and multiple-collector ICP-MS. Chem. Geol. 247, 100–118.

Zhang, H.F., Xu, W.C., Guo, K.Q., Cai, H.M., Yuan, H.L., 2007a. Zircon U–Pb and Hf isotopic composition of deformed granite in the southern margin of the Gangdese belt, Tibet: evidence for early Jurassic subduction of Neo-Tethyan oceanic slab (in Chinese with English abstract). Acta Petrol. Acta 23, 1347–1353.

Zhang, H.F., Xu, W.C., Guo, J.Q., Zong, K.Q., Cai, H.M., Yuan, H.L., 2007b. Indosinian orogenesis of the Gangdise terrane: evidences from zircon U–Pb dating and petrogenesis of granitoids (in Chinese with English abstract). Earth Sci. 32, 155–166.

Zhou, S., Mo, X.X., Dong, G.C., Zhao, Z.D., Qiu, R.Z., Guo, T.Y., Wang, L.L., 2004. ^{40}Ar–^{39}Ar geochronology of Cenozoic Linzizong volcanic rocks from Linzhou Basin, Tibet, China, and their geological implications. Chin. Sci. Bull. 49, 1970–1979.

Zhou, C.Y., Zhu, D.C., Zhao, Z.D., Xu, J.F., Wang, L.Q., Chen, H.H., Xie, L.W., Dong, G.C., Zhou, S., 2008. Petrogenesis of the Daxiong pluton in western Gangdese, Tibet: zircon U–Pb dating and Hf isotopic constraints (in Chinese with English abstract). Acta Petrol. Sin. 24, 348–358.

Zhu, D.C., Pan, G.T., Chung, S.L., Liao, Z.L., Wang, L.Q., Li, G.M., 2008. SHRIMP zircon age and geochemical constraints on the origin of Lower Jurassic volcanic rocks from the Yeba Formation, southern Gangdese, South Tibet. Int. Geol. Rev. 50, 442–471.